Size distribution theory for jumping-droplet condensation

Applied Physics Letters

Size distribution theory for jumping-droplet condensation

Cite as: Appl. Phys. Lett. **114**, 163701 (2019); https://doi.org/10.1063/1.5081053
Submitted: 13 November 2018 . Accepted: 24 March 2019 . Published Online: 24 April 2019

Lenan Zhang, Zhenyuan Xu, Zhengmao Lu, Jianyi Du, and Evelyn N. Wang

Applied Physics Letters ARTICLE scitation.org/journal/apl

Size distribution theory for jumping-droplet condensation

Cite as: Appl. Phys. Lett. **114**, 163701 (2019); doi: 10.1063/1.5081053
Submitted: 13 November 2018 · Accepted: 24 March 2019 ·
Published Online: 24 April 2019

Lenan Zhang,[1,a)] Zhenyuan Xu,[1,2,a)] Zhengmao Lu,[1] Jianyi Du,[1] and Evelyn N. Wang[1,b)]

AFFILIATIONS

[1]Department of Mechanical Engineering, Massachusetts Institute of Technology, 77 Massachusetts Avenue, Cambridge, Massachusetts 02139, USA
[2]Institute of Refrigeration and Cryogenics, Shanghai Jiao Tong University, Shanghai 200240, China

[a)]**Contributions:** L. Zhang and Z. Xu contributed equally to this work.
[b)]enwang@mit.edu

ABSTRACT

Jumping-droplet condensation is promising for various applications where the droplet size distribution plays a key role in the overall system performance. Despite being extensively studied in recent works, inconsistencies existed in previous size distribution models as the droplet growth and removal mechanisms were often not properly described. Here, we developed a theoretical framework where the contact and the coalescence of droplets were identified as the dominant mechanisms for instantaneous size distribution change. We found a critical droplet diameter comparable to the average nucleation site distance, beyond which the droplet population decreased rapidly. This result is analogous to the well-known Fermi-Dirac distribution due to the underlying exclusive principle. We also showed the effect of the contact angle, that is, larger droplets become more probable as surface hydrophobicity increases. The coalescence count distribution given by the current theory agrees well with experimental data. Furthermore, we demonstrated the use of the proposed model in predicting condensation heat transfer coefficients, which also shows good agreement with previous experiments. Our size distribution theory elucidates the fundamental process of droplet growth and interactions leading to an overall size distribution during jumping-droplet condensation, which can be generally applied to self-cleaning, anti-icing/frosting, power generation, and water harvesting.

Jumping-droplet condensation on superhydrophobic surfaces takes advantage of low droplet adhesion and release of excess surface energy, which leads to droplet removal.[1] Accordingly, it has been widely researched for heat transfer enhancement,[2,3] energy conversion,[4] anti-icing/frosting,[5,6] anti-fogging,[7] and self-cleaning.[8] Meanwhile, it is well known that the droplet size distribution is necessary to understand droplet interactions with the solid surface, evaluate the performance of superhydrophobic surfaces, and predict the overall condensation heat transfer coefficients.[9–13] There has been significant theoretical effort in the literature related to droplet interaction dynamics,[14–16] droplet growth,[17–19] superhydrophobic surface fabrication,[2,7,20] and condensation heat transfer enhancement.[3,21–23] However, there lacks a consistent theory that bridges the individual droplet removal mechanism to the collective size distribution of numerous droplets during jumping-droplet condensation.

To understand the underlying physics of droplet size distribution clearly, we explain the droplet growth and removal mechanisms firstly. In dropwise condensation, the droplet growth relies on: (1) coalescence of two or more droplets, resulting in larger size droplets [see the yellow-dashed box in Fig. 1(a)] and (2) direct growth from condensation, which mainly occurs for pre-coalescence of small size droplets [see the red-dashed box in Fig. 1(b)]. Therefore, the small size droplet is typically defined as the droplet with a radius smaller than the coalescence radius. Both small and large size droplets are removed by gravity-induced sweeping. The commonly used size distribution theory established by Le Fevre and Rose considers the coalescence growth and sweeping removal mechanisms [see the yellow-dashed box in Fig. 1(a)].[9,10,24] The population balance theory, on the other hand, was developed to account for the smaller droplets from the direct growth of condensation and the sweeping process characterized by the so-called sweeping period τ [see the small droplets in the red-dashed box in Fig. 1(b) being swept by the large droplet].[13] More recently, these two theories have been combined to map the overall size distribution function through a continuity boundary condition, which has become the widely recognized size distribution theory for dropwise condensation.[12,25–28]

In jumping-droplet condensation, however, the factors that affect the droplet size distribution are fundamentally different in terms of both droplet growth and removal mechanisms. As coalescence leads to

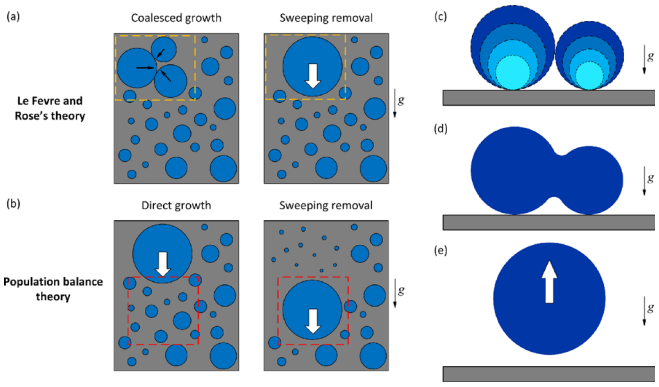

FIG. 1. Schematics of the droplet growth and removal mechanisms for dropwise and jumping-droplet condensation. (a) Coalesced growth and sweeping removal mechanisms considered in Le Fevre and Rose's size distribution theory for dropwise condensation. Large size droplet growth mainly relies on the coalescence of several small droplets [see the yellow-dashed box in (a)] and then removed through gravity driven sweeping. (b) Direct growth and sweeping removal mechanisms incorporated into the population balance theory. Small size droplets directly grow from condensation without coalescence [see the red-dashed box in (b)] and then are swept by larger droplets. (c) Direct growth of droplets on a superhydrophobic surface. (d) Coalescence of two droplets on the superhydrophobic surface. (e) Jumping removal of the coalesced droplet due to the release of excess surface energy. In jumping-droplet condensation, direct growth from condensation is the dominating growth mechanism as the coalescence can lead to jumping removal.

jumping [see Figs. 1(c) and 1(d)], the coalescence-based growth mechanism [see Fig. 1(a)] does not apply, and the direct growth [see Fig. 1(b)] becomes the only droplet growth mechanism for jumping-droplet condensation. On the other hand, the droplet removal is then dominated by the coalescence-jumping process instead of gravity [see Fig. 1(e)].

Although modifications of the population balance theory (MPBT) have been made to adapt the conventional dropwise condensation size distribution theory to jumping-droplet condensation,[27] three major inconsistences exist in the current theory: (1) The coalescence induced jumping removal [see Figs. 1(d) and 1(e)] was not incorporated into the MPBT, i.e., no equations or parameters account for the coalescence induced removal. (2) The droplet population density at the coalescence radius (known as the boundary condition of MPBT) was still given by Le Fevre and Rose's theory,[27] which is only valid for large size droplets in dropwise condensation. Note that in dropwise condensation, the growth of large size droplets mainly relies on the coalescence of several small droplets [see Fig. 1(a)]. However, in jumping-droplet condensation, the majority of large droplets results from direct growth because any coalescence can lead to jumping removal [see Figs. 1(c)–1(e)]. (3) The MPBT has an intrinsic limitation in describing small droplet behavior. The population balance theory, from which the MPBT originates, assumes that there is no coalescence between small droplets as they have little possibility to contact other droplets. However, coalescence can occur at any droplet size range, which is particularly important for jumping-droplet condensation because the droplet size for such conditions is generally small. Therefore, the viability of this assumption needs further evaluation.

In this work, we developed a fundamentally different theory to describe the droplet removal mechanism and the droplet size distribution during jumping-droplet condensation. The droplet population at a certain size is only changed via the contact and the coalescence between droplets and the consequent jumping. We modeled the probability of coalescence for droplets of different sizes, accounting for the properties of superhydrophobic surfaces (contact angle, nucleation site density, distribution and distance) and the geometrical constraints between droplets and nucleation sites. We established the governing equation for the size distribution and found good agreement between the theoretical results and previous experiments.

Our model assumed that: (1) Coalescence induced jumping is the dominant removal mechanism of droplets [see Fig. 2(a)]. Most of the contact and coalescence between two adjacent droplets will trigger the jumping removal process[29–34] (see supplementary material S1 for details). (2) At each moment, two droplet coalescence is the dominant droplet interaction mechanism [see Fig. 2(b)].[14] Note that this assumption excludes only the simultaneous coalescence of multi-droplets (>2). Therefore, in addition to the accurate modeling of two droplet dominant jumping events,[35] it can also describe the condition that two droplets coalesce first and then interact with another droplet before jumping, because this multi-droplet interaction does not occur at the same moment (see supplementary material S1 for details). (3) A quasi-steady state is reached during condensation, i.e., the droplet population density function is independent of time $n(r,t) = n(r)$.[9,10,13,24] (4) Nucleation sites are uniformly distributed on the substrate with an average distance s and the average number of nearest neighbors m.[9,10,12,13,24,26] As an example, the hexagonal distributed nucleation sites have m equal to 6 [see the inset of Fig. 1(b)]. Note that the uniformly distributed nucleation sites can correspond to two conditions. Firstly, nucleation sites can be uniformly patterned arrays, such as hexagonal arrays[10] and square arrays.[12] Secondly, nucleation sites can also be randomly distributed, but the probability density of an arbitrary point on the structured surface to be a nucleation site obeys the uniform distribution.[26] Under both conditions, s and m are functions of spatial distribution of nucleation sites and nucleation density N which describe the statistical behavior of the condensation surface. For example, if nucleation sites are patterned in a uniform hexagonal array, $s = 1.07N^{-0.5}$.[10] If nucleation sites form a uniform square array, $s = N^{-0.5}$.[12] In addition, if the nucleation sites are randomly distributed and the probability density function is a uniform distribution, the nearest neighbors obey the Poisson distribution and $s = 0.5N^{-0.5}$.[26] Therefore, in general, either s or N should be used as the model input, which is the intrinsic property of the substrate and characterized experimentally.

As depicted in Fig. 2(a), the droplet population density $n(r+dr)$ evolves from $n(r)$ with droplet growth. Based on the above assumptions, droplets can either directly grow from r to $r+dr$ (in radius) without coming in contact with any other droplets or coalesce with the nearest neighbors and jump. The first case corresponds to the yellow block marked by (1) in Fig. 2(a). The second case corresponds to the green block marked by (2) in Fig. 2(a), leading to the decrease in n with r. Accordingly, the number balance of droplets growing from radius r to $r+dr$ can be expressed as

$$n(r+dr)dr = n(r)dr - J(r)dr, \tag{1}$$

where $J(r)$ is the frequency of jumping removal at radius r. As any contact between two droplets can lead to jumping removal [assumption (1)], $J(r)$ can be written as

$$J(r) = n(r)p(r), \tag{2}$$

where $p(r)$ represents the probability of the droplet coming in contact with its adjacent droplet when growing from r to $r+dr$. According to

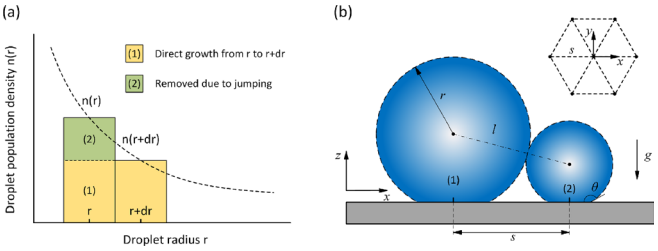

FIG. 2. (a) Schematic of the droplet population density n(r) as a function of droplet radius r. All droplets at radius r + dr arise from the growth of droplets at radius r [see the yellow block marked as (1)]. The droplet population density decreases with radius [see the green block marked as (2)] due to coalescence induced jumping removal. (b) Schematic of two contacting droplets before coalescence (side view). These two droplets are labeled (1) and (2) with a center distance of l. Droplet (1) has a radius of r. The average distance between two adjacent nucleation sites is s, and the apparent contact angle of the droplet is θ. The gravity points to the z-direction. Inset of (b): Hexagonal distribution of nucleation sites shown in the x-y plane (top view).

recent experimental and theoretical observations, the droplet growth rate remains approximately constant for a wide range of droplet radii,[17,19] and most of the droplet interactions occur when two droplets have a similar size.[7] For these two reasons, as shown in Fig. 2(b), to make droplet (1) come in contact with droplet (2) when droplet (1) grows from radius r to $r + dr$, the radius of droplet (2) should be between $l - r - 2dr$ and $l - r$ [l is the center distance between (1) and (2)]. In addition, we should consider that each droplet is surrounded by an average of m droplets due to the nucleation site distribution [see the example nucleation sites in Fig. 2(b)] and eliminate the double counting of the droplet interaction, i.e., (1) interacts with (2) in the same way as (2) interacts with (1). Therefore, if we only consider two droplets' coalescence [assumption (2)], $p(r)$ is explicitly expressed as

$$p(r) = \frac{m}{2}\frac{\int_{l-r-2dr}^{l-r} n(r)dr}{N} \approx m\frac{n(l-r)dr}{N}, \tag{3}$$

where $N = \int_o^\infty n(r)dr$. Incorporating Eqs. (2) and (3) into Eq. (1), we obtained the ordinary functional differential equation for the size distribution function of jumping droplets

$$-\frac{dn(r)}{dr} = m\frac{n(r)n(l-r)}{N}, \tag{4}$$

where l is a function of r which can be calculated according to the geometric constraint if the average distance between two nearest nucleation sites s and the apparent contact angle θ are known [see Fig. 2(b) and Eq. (S1) in supplementary material S2].

We modeled the droplet size distribution and the corresponding number of coalescence events for two different advancing contact angles ($\theta = 90°$ and 180°, respectively). Note that, in practice, the $\theta = 90°$ case can never give rise to jumping-induced removal, and it is simply studied to show the effect of wettability. When $\theta = 90°$, $l = s$, and therefore, Eq. (4) can consequently be simplified, providing physical insights into the droplet size distribution. When $\theta = 180°$, which is the other extreme case, l becomes a function of r. In addition, we found that the solution to $\theta = 180°$ is a good approximation to the droplet size distribution when $\theta > 150°$, which can be widely used for a variety of superhydrophobic conditions (see supplementary material S2 for analysis). In this work, the droplet number density was normalized by its maximum and the droplet radius was normalized by $a = s/2$.

When $\theta = 90°$, Eq. (4) can be solved analytically (see supplementary material S3 for the derivation) where the normalized droplet size distribution function is given by

$$n^*(r^*) = \frac{1}{\exp(6(r^* - 1)) + 1}, \tag{5}$$

where $r^* = r/a$ is the normalized droplet radius. As shown in Fig. 3(a), $n^*(r^*)$ behaves like a sigmoid function when $\theta = 90°$. The droplet population is initially large when r^* is small, but decreases rapidly when $r^* \approx 1$ and finally approaches 0 as $r^* \to \infty$. Smaller droplets ($r^* < 1$) contribute more to the total population because they are less likely to come in contact with their nearest neighbors. On the contrary, large droplets ($r^* > 1$) are more probable to contact adjacent droplets and then are removed through coalescence induced jumping. As a result, the population of very large droplets remaining on the surfaces is very low [see Fig. 3(a)].

More interestingly, note that Eq. (5) resembles the well-known Fermi-Dirac distribution with the chemical potential of 1 (also known as the sigmoid's midpoint). According to statistical mechanics, the Fermi-Dirac distribution is governed by the Pauli exclusive principle, which states that two or more identical particles cannot occupy the same state. Fundamentally, the droplet interaction mechanism is analogous to the Pauli exclusive principle: two droplets larger than a in radius cannot occupy the adjacent nucleation sites simultaneously. Otherwise, both of them will jump off the surface due to the geometric constraint of the nucleation site distance s [see the inset of Fig. 3(b)].

When $\theta = 180°$, using the zeroth-order approximation, we can also find the analytical solution (see supplementary material S4 for the derivation) as

$$n^*(r^*) = \exp\left(-e\left(Ei\left(-\frac{1}{r^*}\right) + r^*\exp\left(-\frac{1}{r^*}\right)\right)\right), \tag{6}$$

where $Ei(x) = -\int_{-x}^{\infty}\exp(-t)dt/t$ is the exponential integral function. As shown in Fig. 3(a), the general trend of the size distribution function at $\theta = 180°$ is the same as that at $\theta = 90°$ because both of them are governed by the same droplet removal mechanism. However, the size distribution curve shifts to the right at a large r^*, indicating that the number of large droplets with $r^* > 1$ increases with the increase in surface hydrophobicity. To explain this trend, we consider the geometric constraint to the droplet size again. The maximum radius of a droplet on a single nucleation site is determined by l, which monotonically increases with the contact angle [see Fig. 1(b) and supplementary material S2 for details]. Specifically, when $\theta = 90°$, $l \equiv s$ and the droplet radius larger than s is then not allowed [the droplet size population becomes zero when $r^* \geq 2$ in Fig. 3(a)]. When θ increases to 180°, however, l becomes a function of droplet radius, and is always larger than s (see supplementary material S2 for the explanation of the droplet size distribution function with $\theta = 180°$ deviating from the standard sigmoid function). Consequently, large size droplets become more probable on the superhydrophobic surfaces. Additionally, a higher order accuracy solution at $\theta = 180°$ is given numerically by iterating the zeroth-order solution into Eq. (4) and solving the corresponding boundary value problem (see supplementary material S4 for details), and the deviation caused by the zeroth-order approximation is small as shown in Fig. 3(a). To validate our model, the theoretical curves were then compared with various

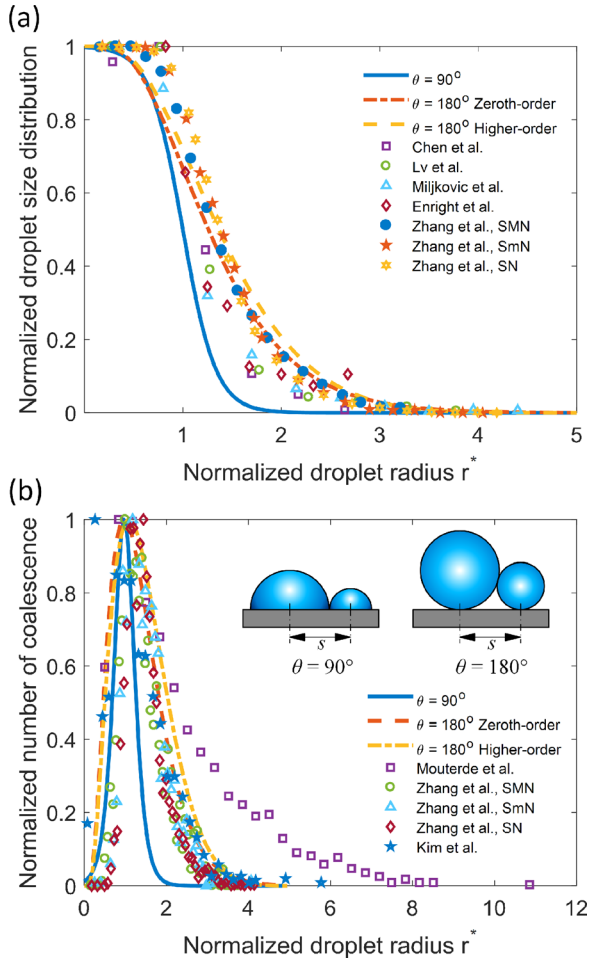

FIG. 3. (a) Normalized droplet size distribution as a function of dimensionless droplet radius. The droplet radius is normalized by a = s/2, i.e., $r^* = r/a$. The droplet size distribution curve behaves like a sigmoid function where the population of droplets decreases significantly when r > a. When the contact angle increases, the distribution curve shifts to the right, indicating the existence of more large size droplets [see Eq. (S3) and relevant discussions in supplementary material S2]. (b) Normalized number of coalescence events as a function of normalized droplet radius. The peak of the coalescence number appears at around r = a, indicating that most coalescence occurs when two adjacent droplets have a similar size. For $\theta = 90°$, the number of coalescence events is a Gaussian distribution centered at $r^* = 1$. The theoretical curves were compared with various experimental results on both regular patterned and random structured surfaces and show good agreement in general.[2,7,26,34,36–38] In Zhang *et al.*'s work, SMN, SmN, and SN represent the high density and the big size of microstructures, the low density and the small size of microstructures, and the absence of microstructures, respectively.[36] The average distance between the nearest neighbors s (for Lv *et al.*,[37] Mouterde *et al.*,[7] and Kim *et al.*'s[38] works) or nucleation density N (for Miljkovic *et al.*,[2] Enright *et al.*,[26] and Zhang *et al.*'s[36] works) was used as the model input, which was characterized by corresponding experiments.[2,7,26,34,36–38] Inset: Schematic of two contacting droplets with 90° and 180° contact angles, respectively.

experimental results on both regular patterned[7,34] and random structured[2,26,36–38] superhydrophobic surfaces. The average distance between the nearest neighbors s[7,37,38] or the nucleation density N[2,26,36] characterized by these works were used as the model input. As shown in Fig. 3(a), all experimental data follow the same trend as our theoretical prediction. Specifically, most of the data points are between $\theta = 90°$ and $\theta = 180°$ curves, mainly because the droplet contact angle of these experiments is smaller than 180° and the population of small size droplets is typically underestimated due to the limitation of microscope spatial resolution.

As the change in the droplet population arises from coalescence only, we can easily obtain the number of coalescence events by taking the derivative to the droplet size distribution function [see Eq. (1)]. As shown in Fig. 3(b), the number of coalescence events first increases with the droplet radius and then drops gradually. The number of coalescence events for small droplets ($r < a$) is low because smaller droplets have less opportunities to contact the adjacent droplets. Although large size droplets ($r > a$) are more likely to coalesce with their nearest neighbor, the total population of large size droplets is small resulting in a low number of coalescence events at very large r. We also observed that the number of coalescence events peaks at around $r = a$, which indicates that most of the coalescence occurs when the size of two droplets is comparable. This is consistent with previous experimental observations that the most frequent jumping directions are close to the vertical direction (induced by the coalescence of two droplets with similar size).[1,14,39] However, prior condensation theories, in general, could not predict the broad line shape of the number of coalescence events.[2,9,10,13,24] To further assess the results, we compared the theory with experimental jumping event statistics,[7,36,38] where good agreement was found in general [Fig. 3(b)]. Slight discrepancies can be seen between the theory and the experimental results of Zhang *et al.*,[36] when $r < 0.5a$ which might arise from the simplification of assumption 1 and the underestimation of small droplets jumping events due to the limitation of the microscope's spatial resolution. There is an unusual case that when $r > 3a$, the discrepancy between the theory and Mouterde *et al.*'s experiment is relatively large.[7] Since the size of the jumping-droplet (with a coalescence radius of 2–3 μm) in Mouterde *et al.*'s work is relatively small compared to common conditions due to the surface properties,[7] the jumping events of very small droplets might be underestimated, which leads to this discrepancy after normalization.

To further demonstrate the significance of the proposed size distribution theory, we compared the present work [see T1 in Fig. 4(a)] with the MPBT [see T2 in Fig. 4(a)] under various nucleation density conditions (see supplementary material S5 for detailed calculations). The MPBT predicts that the number of large size droplets is more than that of the small size droplets [see Fig. 4(a)], which is inconsistent with previous experimental observations.[2,7,26] In theory, the population of large size droplets should always be smaller than that of small size droplets because all of the large size droplets originate from small size droplets through a direct growth mechanism [see Figs. 1(b) and 1(c)]. To show a possible application of the proposed theory, we calculated the overall heat transfer performance of jumping-droplet condensation on the silanated copper oxide nanostructured surface at different subcooling temperatures from 0.5 °C to 5 °C [see Fig. 4(b) and supplementary material S5]. The nucleation density N is 5×10^{10} m^{-2}, which was experimentally characterized by Enright *et al.*[26] on the same surface. The overall surface heat flux q'' is given by

$$q'' = \int Q_d(r) n(r) dr, \tag{7}$$

where $Q_d(r)$ is the single droplet heat transfer rate given by the droplet growth theories,[18,19] and $n(r)$ can be obtained from $n^*(r^*)$ by

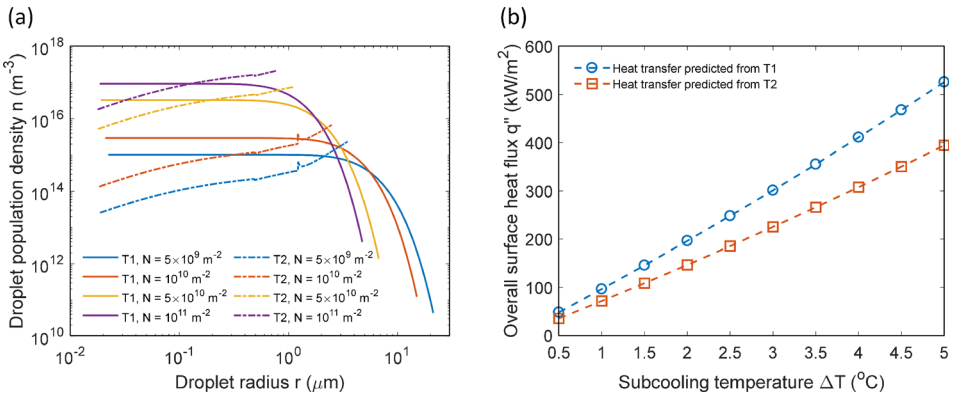

FIG. 4. (a) Droplet size distribution under different nucleation density N calculated by the proposed theory (T1) and the MPBT (T2). The singular point shown in T2 is due to an intrinsic numerical problem of MPBT (see supplementary material S5 for a detailed discussion). (b) Overall surface heat transfer performance of jumping-droplet condensation on silanated copper oxide nanostructured surfaces predicted by the proposed theory and the MPBT. The predicted HTC from the present theory is ≈100 kW/m^{2}K, closer to the experimental results (≈92 kW/m^{2}K) than the ≈75 kW/m^{2}K from the MPBT.

considering the conservation of total droplet population, i.e., $N = \int n(r)dr$ (see supplementary material S5 for detailed calculations). The heat transfer coefficient (HTC) predicted by the present theory is ≈100 kW/m^{2}K, which is significantly closer to the experimental results (≈92 kW/m^{2}K)2 compared to the MPBT prediction (≈75 kW/m^{2}K) [see Fig. 4(b)]. The MPBT underestimates the overall heat transfer because the population of small size droplets, which shows better heat transfer performance, is underestimated [see Fig. 4(a)].

In conclusion, we elucidated the underlying physics of the droplet size distribution theory for jumping-droplet condensation. We developed the governing equation and showed the "sigmoid function" like droplet size distribution due to the intrinsic exclusive property of the droplet removal mechanism. We analyzed the effect of contact angles, which influences the corresponding number of coalescence events taking place at different droplet radii. As an application, the proposed theory was used to estimate the overall heat transfer performance of jumping-droplet condensation. With the experimentally characterized nucleation density, the heat transfer coefficient predicted by the proposed theory agrees well with the experimental studies. This work not only provides physical insights into droplet interaction during jumping-droplet condensation, but can be generally useful for superhydrophobic surface design and condensation heat transfer enhancement.

See supplementary material for more information on theoretical derivations, further discussion and data analysis.

L. Zhang gratefully acknowledges funding support from the MIT/MTL GaN Energy Initiative and the Singapore-MIT Alliance for Research and Technology (SMART) LEES Program. Z. Xu acknowledges funding support from National Natural Science Foundation of China (Grant No. 51606124). Z. Lu acknowledges funding support from the Air Force Office of Scientific Research with Dr. Ali Sayir as the program manager under Award No. FA9550-15-1-0310.

REFERENCES

[1]J. B. Boreyko and C.-H. Chen, Phys. Rev. Lett. **103**, 184501 (2009).
[2]N. Miljkovic, R. Enright, Y. Nam, K. Lopez, N. Dou, J. Sack, and E. N. Wang, Nano Lett. **13**, 179 (2013).
[3]R. Wen, Q. Li, J. Wu, G. Wu, W. Wang, Y. Chen, X. Ma, D. Zhao, and R. Yang, Nano Energy **33**, 177 (2017).
[4]K. F. Wiedenheft, H. A. Guo, X. Qu, J. B. Boreyko, F. Liu, K. Zhang, F. Eid, A. Choudhury, Z. Li, and C.-H. Chen, Appl. Phys. Lett. **110**, 141601 (2017).
[5]Q. Zhang, M. He, J. Chen, J. Wang, Y. Song, and L. Jiang, Chem. Commun. **49**, 4516 (2013).
[6]J. B. Boreyko and C. P. Collier, ACS Nano **7**, 1618 (2013).
[7]T. Mouterde, G. Lehoucq, S. Xavier, A. Checco, C. T. Black, A. Rahman, T. Midavaine, C. Clanet, and D. Quéré, Nat. Mater. **16**, 658 (2017).
[8]K. M. Wisdom, J. A. Watson, X. Qu, F. Liu, G. S. Watson, and C.-H. Chen, Proc. Natl. Acad. Sci. **110**, 7992 (2013).
[9]J. W. Rose, Int. J. Heat Mass Transfer **19**, 1363 (1976).
[10]J. W. Rose and L. R. Glicksman, Int. J. Heat Mass Transfer **16**, 411 (1973).
[11]H. Tanaka and S. Hatamiya, Proc. 8th Int. Heat Transf. Conf. **4**, 1671 (1986).
[12]S. Kim and K. J. Kim, J. Heat Transfer **133**, 081502 (2011).
[13]H. W. Wen and R. M. Jer, Chem. Eng. J. **12**, 225 (1976).
[14]R. Enright, N. Miljkovic, J. Sprittles, K. Nolan, R. Mitchell, and E. N. Wang, ACS Nano **8**, 10352 (2014).
[15]X. Liu, P. Cheng, and X. Quan, Int. J. Heat Mass Transfer **73**, 195 (2014).
[16]Q. Zhang, D. Sun, Y. Zhang, and M. Zhu, Langmuir **30**, 12559 (2014).
[17]N. Miljkovic, R. Enright, and E. N. Wang, ACS Nano **6**, 1776 (2012).
[18]L. Zhang, J. Zhu, K. L. Wilke, Z. Xu, L. Zhao, Z. Lu, L. L. Goddard, and E. N. Wang, ACS Nano **13**, 1953 (2019).
[19]Z. Xu, L. Zhang, K. Wilke, and E. N. Wang, Langmuir **34**, 9085 (2018).
[20]M. He, Y. Ding, J. Chen, and Y. Song, ACS Nano **10**, 9456 (2016).
[21]R. Wen, S. Xu, X. Ma, Y.-C. Lee, and R. Yang, Joule **2**, 269 (2018).
[22]D. J. Preston and E. N. Wang, Joule **2**, 205 (2018).
[23]X. Qu, J. B. Boreyko, F. Liu, R. L. Agapov, N. V. Lavrik, S. T. Retterer, J. J. Feng, C. P. Collier, and C.-H. Chen, Appl. Phys. Lett. **106**, 221601 (2015).
[24]E. J. Le Fevre and J. W. Rose, 3rd Int. Heat Transfer Conf. **2**, 362 (1966).
[25]M. Abu-Orabi, Int. J. Heat Mass Transfer **41**, 81 (1998).
[26]R. Enright, N. Miljkovic, N. Dou, Y. Nam, and E. N. Wang, J. Heat Transfer **135**, 091304 (2013).
[27]N. Miljkovic, R. Enright, and E. N. Wang, J. Heat Transfer **135**, 111004 (2013).
[28]S. Chavan, H. Cha, D. Orejon, K. Nawaz, N. Singla, Y. F. Yeung, D. Park, D. H. Kang, Y. Chang, Y. Takata, and N. Miljkovic, Langmuir **32**, 7774 (2016).
[29]F.-F. Xie, G. Lu, X.-D. Wang, and D.-Q. Wang, Langmuir **34**, 11195 (2018).
[30]S. Gao, Q. Liao, W. Liu, and Z. Liu, J. Phys. Chem. Lett. **9**, 13 (2018).
[31]Z. Liang and P. Keblinski, Appl. Phys. Lett. **107**, 143105 (2015).
[32]F. Liu, G. Ghigliotti, J. J. Feng, and C.-H. Chen, J. Fluid Mech. **752**, 39 (2014).
[33]H. Cha, C. Xu, J. Sotelo, J. M. Chun, Y. Yokoyama, R. Enright, and N. Miljkovic, Phys. Rev. Fluids **1**, 064102 (2016).
[34]X. Chen, J. A. Weibel, and S. V. Garimella, ACS Omega **2**, 2883 (2017).
[35]M. D. Mulroe, B. R. Srijanto, S. F. Ahmadi, C. P. Collier, and J. B. Boreyko, ACS Nano **11**, 8499 (2017).
[36]P. Zhang, Y. Maeda, F. Lv, Y. Takata, and D. Orejon, ACS Appl. Mater. Interfaces **9**, 35391 (2017).
[37]C. Lv, P. Hao, Z. Yao, and F. Niu, Langmuir **31**, 2414 (2015).
[38]M.-K. Kim, H. Cha, P. Birbarah, S. Chavan, C. Zhong, Y. Xu, and N. Miljkovic, Langmuir **31**, 13452 (2015).
[39]D. J. Preston, N. Miljkovic, E. N. Wang, and R. Enright, J. Heat Transfer **136**, 080909 (2014).